



Improving Forest Height-To-Biomass Allometry With Structure Information: A Tandem-X Study

Changhyun Choi, Matteo Pardini , *Member, IEEE*, Michael Heym,
and Konstantinos P. Papathanassiou , *Fellow, IEEE*

Abstract—Allometric relations that link forest above ground biomass to top forest (i.e., canopy) height are of particular significance in the context of lidar and interferometric synthetic aperture radar remote sensing, as both techniques allow accurate height measurements at ecologically relevant spatial scales. Besides the often unknown allometry itself, its spatial variation in heterogeneous forest environments restricts the performance when using a single fixed height-to-biomass allometric relation. This paper addresses how forest structure information derived from interferometric TanDEM-X data can be used to locally adapt the height-to-biomass allometry in heterogeneous forests, and to improve biomass estimation performance. The analysis is carried out using TanDEM-X interferometric measurements in three tropical forest test sites in Gabon. A structure index expressing forest density is derived from the TanDEM-X data. Then, a continuous relationship between the structure index and the allometric level that defines the forest height-to-biomass allometry is reconstructed from the available lidar data, and used to vary the height-to-biomass relationship. Finally, the potential of the derived structure index to support an allometric relationship common to all sites is evaluated. The experimental results show the appropriateness of TanDEM-X data for characterizing structure and in this way improving the biomass estimation performance.

Index Terms—Above-ground biomass, forest height, forest structure, interferometry, synthetic aperture radar (SAR), tandem-X.

I. INTRODUCTION

B IOMASS has a direct relationship to carbon content and is a measure of forest and ecosystem productivity. Estimation of biomass is very inaccurate at local, regional and supra-regional scales. Ground measurements of biomass in natural forests often exhibit errors much greater than 20%. Particularly large are the deviations in tropical and natural forests due to their spatial heterogeneity. Dynamic changes of biomass and their spatial distribution are a direct measure of the exchange

Manuscript received November 15, 2020; revised May 28, 2021; accepted September 3, 2021. Date of publication September 29, 2021; date of current version October 25, 2021. (*Corresponding author: Matteo Pardini.*)

Changhyun Choi is with Microwaves and Radar Institute, German Aerospace Center, Wessling 82234, Germany, and also with the Institute of Environmental Engineering, Swiss Federal Institute of Technology Zurich, 8093 Zurich, Switzerland (e-mail: changhyun.choi@dlr.de).

Michael Heym is with the Bavarian State Institute of Forestry (Bayerische Landesanstalt für Wald und Forstwirtschaft), 85354 Freising, Germany (e-mail: michael.heyms@lrz.tu-muenchen.de).

Matteo Pardini and Konstantinos P. Papathanassiou are with Microwaves and Radar Institute, German Aerospace Center, 82234 Wessling, Germany (e-mail: matteo.pardini@dlr.de; kostas.papathanassiou@dlr.de).

Digital Object Identifier 10.1109/JSTARS.2021.3116443

of carbon between the terrestrial ecosystem and the atmosphere [1]. At the same time, they characterize the variation of forest growth and productivity induced by water or climate stress [2].

The above ground biomass (AGB) B_T of a single tree can be expressed as the product of the tree volume V with its (species specific) wood density ρ [3], [4]. Different adequate standards of tree volume can be chosen depending on the individual application. In forestry, the focus on the dominant stem contribution suggests the use of stem volume that leads to

$$B_T = V \cdot \rho = F \cdot \left(\frac{\pi D^2}{4} \right) \cdot H \cdot \rho \quad (1)$$

where D is the stem diameter at breast height (also known as DBH), H is the tree height, and F is a factor that accounts for the shape of the stem [3], [4]. Accounting for the total tree volume including its leaves and branches is more common for ecological applications and carbon stock estimates.

However, the use of (1) in the context of remote sensing is rather limited to high resolution airborne implementations because the spatial resolution of conventional and especially spaceborne configurations does not allow us to measure single tree parameters. With a typical spatial resolution on the order of few to ten meters, such configurations can provide forest parameter estimates at some tenths of meters, representative of patches of trees or forest stands rather than of single trees. However, the transition of (1) from a single tree to a stand biomass relation by replacing the individual tree parameters with the stand means (e.g., mean forest height, mean diameter or alternatively basal area, and mean wood density) is not straightforward and strongly depends on the stand density and heterogeneity in terms of species and age composition [5], [6].

The potential of either spaceborne lidar or interferometric synthetic aperture radar (InSAR) configurations to measure forest height at spatial scales of 1 hectare (ha) or even below motivated the use of the so-called forest height-to-biomass allometry at stand level. The AGB B is expressed in terms of (top) height by means of an exponential relationship [4]–[8]

$$B = \alpha_0 \cdot H^{\beta_0} \quad (2)$$

where H is the maximum height within the stand area equivalent to the top canopy height, and (α_0, β_0) , are the so-called allometric factor and reference (allometric) exponent, respectively. The reference exponent β_0 defines the underlying allometric relation accounting for species composition and growing conditions of



Fig. 1. Three depicted forest stands have the same top height H . Their horizontal density decreases from left to right. The height axis is referred to the ground, which is located in its origin (0 m).

a certain stand. The allometric factor accounts then for (anthropogenic and natural) density variations across stands of the same composition. When the reference exponent β_0 is fixed, α_0 is also known as the allometric level as it scales a set of height-to-biomass relations with the same reference exponent accounting for different stand densities (e.g., different basal areas at a given age) or stand ages. A successful implementation requires the two allometric parameters to be either *a priori* known or estimated from reference (for example inventory) measurements. Indeed, allometric relationships in form of (2) have been successfully used to derive biomass estimates from height estimates [6]–[11], however for rather homogeneous stand and forest conditions.

However, the spatial variability in stand density and/or structure reduces the performance of a single height-to-biomass relation with fixed α_0 and β_0 . Accordingly, in spatially heterogeneous (in terms of density and structure) forests a fixed height-to-biomass allometry leads to a poor performance or even breaks down [4]–[6], [9]. To visualize this insufficiency three stands with the same H are depicted in Fig. 1. The tree density decreases from left to right with the stand biomass to decrease accordingly. In this particular case, if only height is used and (α_0, β_0) are fixed, the same biomass is estimated across the three stands. Using allometric parameters (α_0, β_0) fitting the denser stand will overestimate the biomass in the sparser stand, and vice versa.

Summarizing, two main factors limit the use of the height-to-biomass allometry in a wide context: (i) the large uncertainty in the knowledge of the allometric parameters (α_0, β_0) for the individual forest conditions (arising from the insufficiency or complete lack of appropriate reference measurements), and (ii) the inability to adapt (α_0, β_0) to the spatial variability of forests.

However, today both limitations appear less restrictive making a revisit of the height-to-biomass allometry attractive. Terrestrial lidar scanning (TLS) techniques have the potential to make plot inventory measurements more accurate and faster [12]. At the same time, spaceborne waveform lidar configurations sample forest height in a more or less dense grid, and provide a set of waveform metrics that allow us to estimate AGB (using empirically derived models) [13], [14]. TLS and/or spaceborne waveform lidars are able to provide enough forest height and biomass measurements to define a general height-to-biomass allometry at regional or even finer scales. Hence, they resolve, at least to a large extent, the first limitation. On the other hand, the spatial variability of allometry can be accounted with remote sensing configurations able to estimate not only forest height,

but also forest structure information with a subhectare spatial resolution. Indeed, SAR interferometry [15]–[21] and especially SAR tomography have been proven to be able to characterize physical forest structure, the latter relying on the reconstruction of the three-dimensional (3-D) radar reflectivity [22]–[25].

The open question is how far the knowledge of forest structure can be used to adapt (and improve) the general height-to-biomass allometry to local scales. This paper addresses this question in the context of TanDEM-X (i.e., bistatic interferometric acquisitions at X-band) and waveform lidar measurements. Height and biomass estimates from the waveform lidar measurements are used to establish a general height-to-biomass allometry. Then, the horizontal structure index HS as defined in [24] is reconstructed from TanDEM-X measurements and used to account for the spatial variability (by means of the allometric level) of the height-to-biomass allometry within the test site

$$B = \alpha(\text{HS}) \cdot H^{\beta_0}. \quad (3)$$

There are two arguments for using HS to adapt α : first, its relation to the well-established stand density index [26] (and thus to basal area) as discussed and demonstrated in [24], and second, the ability to obtain HS estimates from TanDEM-X data.

Accordingly, in the following sections, the estimation of H and HS from TanDEM-X data, the performance of conventional height-to-biomass allometry and the use of HS to improve the height-to-biomass allometry performance for different tropical forest types and conditions are discussed.

II. TEST SITES AND DATASET

A. Test Sites

The AfriSAR campaign was carried out over tropical forest sites in Gabon in 2015 and 2016 [27], [28]. The objective of the campaign was to acquire air- and space-borne polarimetric SAR interferometric and tomographic data sets complemented by airborne waveform lidar [28] and field measurements [29] for the development and validation of forest height, structure and biomass estimation algorithms. Three of the AfriSAR sites are considered in this article: Lopé; Mabounie; and Mondah. Their locations are shown in Fig. 2.

The Lopé site is located within the Lopé National Park near the geographic center of Gabon. The site consists of a variety of structure types ranging from open savannas to undisturbed tall (sometimes exceeding 50 m) dense forest stands. Colonizing forest (sparse forest stands mixed up with savanna) or monodominant Okoume (dense, monolayered, tall and dense forest stands) are two particular cases [29]–[31]. Biomass ranges between 10 t/ha in savanna areas and 600 t/ha in dense forest areas. The terrain is hilly with many local slopes steeper than 20°.

The Mabounie site is part of the “Maboumine” mining project started in 2005. The site is covered by mature stands with canopy heights between 40 to 60 m and biomass levels up to 400 t/ha, but is signed by local degradation caused by roads, buildings, and other infrastructure. The site includes also partially flooded areas containing swamp mixed forest [28].

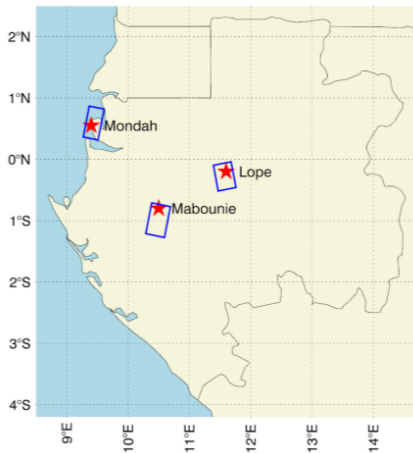


Fig. 2. Locations of the three selected AfriSAR test sites (red stars) and TanDEM-X acquisitions (blue rectangles) in Gabon (central Africa).

Finally, Mondah is a partially flooded area containing mangrove and mahogany woodlands in northwest Gabon. The western part is a primary forest taller than 50 m, with dense and homogenous stands while the eastern part is secondary forest [28]. The topography is fairly flat within the site.

B. Lidar Acquisitions

Waveform lidar data were acquired by NASA's land and vegetation and ice sensor (LVIS) in February and March 2016 [28], [32], [33]. During AfriSAR, LVIS was operated at a nominal flight altitude of 24 000 ft (equivalent to 7315 m), and acquired data with partially overlapping footprints on ground with an average diameter around 22 m [28].

For each test site, the digital terrain model (DTM) and relative height (RH) metrics were derived from the waveforms [33]. Each RH metric expresses the height above ground at which a certain percentage of the total waveform energy is received [14]. For instance, the RH100 represents to the height above the ground in which the total energy is received. RH metrics have been used to estimate biomass and to describe the canopy vertical structure [13], [14].

In the following, the RH100 is considered as the top canopy height within a footprint, and is used as a reference for the validation of the heights estimated from TanDEM-X coherences. Consistently with the formulation in Section I, the LVIS top height H_{LVIS} has been calculated by taking the maximum RH100 for every 1 ha resolution cell on ground.

Similarly, the waveform-derived AGB estimates B_{LVIS} and their uncertainty at 1 ha resolution, estimated by means of an allometric relationship linking height and RH metrics to the LVIS AGB and parameterized by using the available field inventory plots, have been used as reference [28], [34]. An overall root mean square error around 70 t/ha across all inventory plots was documented [28], [34]. LVIS RH and biomass data sets are ideal for the experiments in this article as they cover large areas allowing to appreciate structure gradients, and provide a statistically (very) large number of samples for comparison at the desired 1 ha resolution.

TABLE I
SUMMARY OF TANDEM-X ACQUISITIONS PARAMETERS

Test Site	Lopé	Mabounie	Mondah
Acquisition Date	Jan. 25, 2016	Oct. 5, 2015	Nov. 11, 2015
Frequency	X-band		
Polarization	HH		
Ground resolution (Range / Azimuth)	1.95 m / 1.99 m	2.26 m / 2.05 m	1.84 m / 1.87 m
Vert. wavenumber	$\sim 0.10 \text{ m}^{-1}$	$\sim 0.078 \text{ m}^{-1}$	$\sim 0.062 \text{ m}^{-1}$
HoA	$\sim 62.8 \text{ m}$	$\sim 80.5 \text{ m}$	$\sim 101.3 \text{ m}$
Incidence angle	44.5°	37.1°	47.7°

Fig. 3 shows the maps of H_{LVIS} and B_{LVIS} for the three selected sites. The largest continuous LVIS coverage is over Lopé. H_{LVIS} is larger than 50 m in the northwestern part and lower in the southeastern part, but overall without relevant spatial gradients. At the same time, B_{LVIS} varies significantly stronger suggesting a likewise significant structure dependency. In Mabounie, many footprints are lost because of cloud coverage. In Mondah, the short stands ($H_{LVIS} < 30 \text{ m}$) in the central part of the scene have a low biomass ($B_{LVIS} < 100 \text{ t/ha}$). In contrast, in the western part B_{LVIS} can reach up to 700 t/ha for the taller primary stands (H_{LVIS} around 50 m).

C. TanDEM-X Acquisitions

Single-polarimetric stripmap bistatic TanDEM-X data were acquired close in time to the LVIS flights. The relevant acquisition parameters are given in Table I. For every data set the InSAR complex coherence has been calculated as

$$\gamma(\kappa_z) = \frac{\langle S_1 \cdot S_2^* \rangle}{\sqrt{\langle S_1 \cdot S_1^* \rangle \langle S_2 \cdot S_2^* \rangle}} \quad (4)$$

where S_1 and S_2 are single-look complex amplitudes of the two images, and $(\cdot)^*$ and $\langle \cdot \rangle$ denote the complex conjugation and the spatial averaging operators. For forest height estimation, the spatial averaging has been performed using cells measuring $25 \text{ m} \times 25 \text{ m}$ (corresponding to ~ 150 independent looks) in ground range – azimuth, respectively. For the estimation of the horizontal structure index (see Section IV-B) a finer resolution of $10 \text{ m} \times 10 \text{ m}$ (corresponding to 25 independent looks) has been chosen. Finally, biomass, horizontal structure index and top height have been calculated at the scale of 1 ha ($100 \text{ m} \times 100 \text{ m}$), consistent to the reference lidar data.

In (4), κ_z represents the vertical wavenumber, which expresses the sensitivity (i.e., the derivative) of the InSAR phase difference with respect to (vertical) height [35], [36]. For the bistatic mode

$$\kappa_z = \frac{2\pi}{\text{HoA}} \cong \frac{2\pi}{\lambda} \frac{B_\perp}{R \sin \theta_i} \quad (5)$$

where HoA is the InSAR Height Of Ambiguity, B_\perp is the perpendicular InSAR baseline, λ is the radar wavelength, and R is the slant range distance. θ_i is the slope-corrected incidence angle, which corresponds to the difference between the incidence angle and the local terrain slope in range direction. The terrain slopes

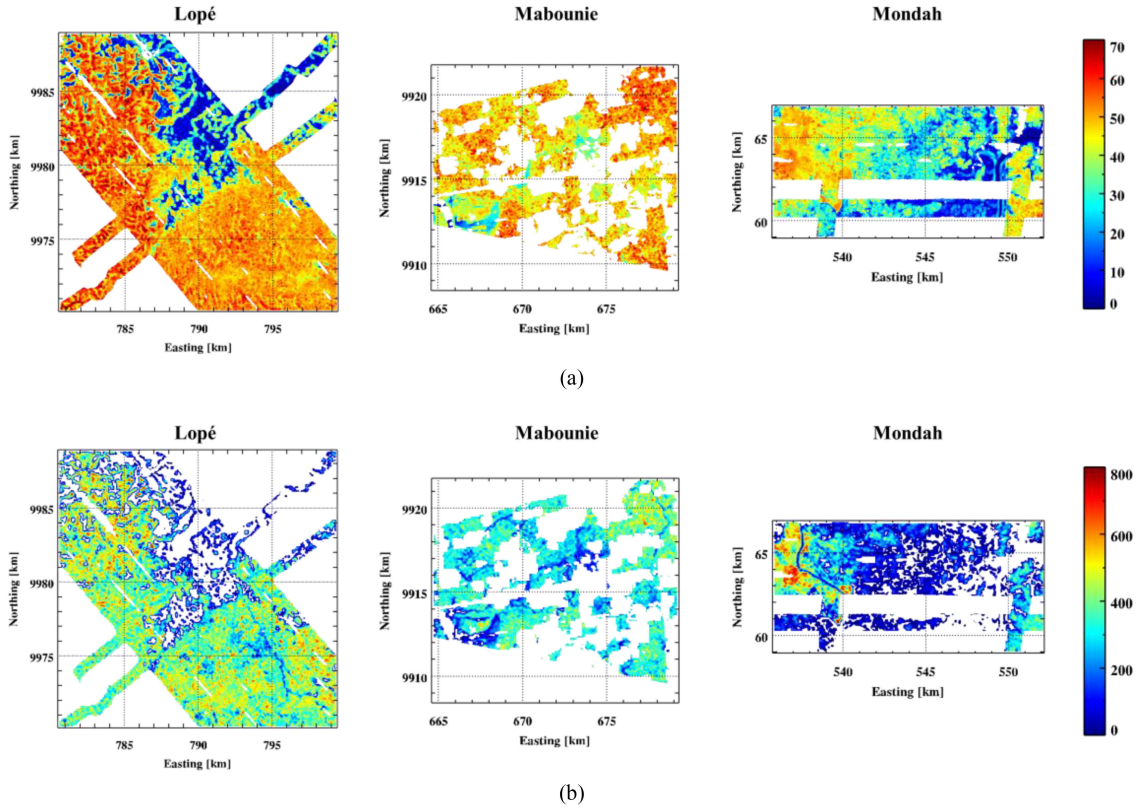


Fig. 3. (a) LVIS top height (H_{LVIS}) maps in meters (m), and (b) AGB (B_{LVIS}) maps in tons per hectare (t/ha) for Lopé, Mabounie, and Mondah. All maps are in UTM coordinates and their resolution is $100\text{ m} \times 100\text{ m}$ in easting and northing direction. The coverage in Lopé is around 19 km (easting) by 19 km (northing), in Mabounie is $15\text{ km} \times 13\text{ km}$, and in Mondah is $16\text{ km} \times 8\text{ km}$.

have been calculated using the TanDEM-X digital elevation model (DEM). The vertical wavenumber characterizes also the performance of parameter inversion from InSAR coherence measurements. In the case of forest height estimation, one single κ_z allows unbiased and accurate inversion only for a limited range of forest heights [36]. In Lopé a mean κ_z of 0.1 rad/m leads to an optimum performance range of 15 to 40 m appropriate to cover most of the forest height in the scene, however with some (significant) loss of performance for the tallest stands with height close to the HoA (around 62 m), far above the optimum performance range. For Mabounie and Mondah, the κ_z values are lower, increasing further the HoA and shifting the optimum performance range to larger heights.

For bistatic acquisitions, the absence of temporal decorrelation leaves signal-to-noise ratio (SNR) decorrelation γ_{SNR} , range (spectral) decorrelation $\gamma_{rg}(\kappa_z)$, quantization decorrelation γ_Q and volume decorrelation $\gamma_{Vol}(\kappa_z)$ as the remaining decorrelation contributions [35]

$$\gamma(\kappa_z) = \gamma_{SNR} \cdot \gamma_{rg}(\kappa_z) \cdot \gamma_Q \cdot \gamma_{Vol}(\kappa_z). \quad (6)$$

Height is estimated from $\gamma_{Vol}(\kappa_z)$ obtained from $\gamma(\kappa_z)$ after compensating all the other contributions. γ_{SNR} and $\gamma_{rg}(\kappa_z)$ have been calculated and compensated using the procedure described in [35]. A fixed value of 0.97 was assumed for γ_Q according to the analysis in [37].

III. FOREST BIOMASS ESTIMATION FROM TANDEM-X HEIGHT

A. Forest Height Inversion

After coherence calibration (see Section II-C), the vertical reflectivity function (i.e., the vertical distribution of scatterers) underlying $\gamma_{Vol}(\kappa_z)$ is usually represented by a two-layer model accounting for the ground and volume (back-) scattering contributions. However, at X-band and for dense(r) forest conditions, the ground contribution is often neglected so that [35], [36], [38]

$$\gamma_{Vol}(\kappa_z) = \exp(i\phi_0) \cdot \gamma_V(\kappa_z). \quad (7)$$

The phase term $\phi_0 = \kappa_z z_0$ is the InSAR phase corresponding to the ground height z_0 and

$$\gamma_V(\kappa_z) = \frac{\int_0^{h_V} f_V(z) \exp(i\kappa_z Z) dz}{\int_0^{h_V} f_V(z) dz} \quad (8)$$

where $f_V(z)$ is the volume-only vertical reflectivity function and h_V is the top volume (i.e., forest) height with respect to the ground topography. For $f_V(z)$ an exponential distribution of scatterers is widely used [35], [36], [38]

$$f_V(z) = \exp\left[\frac{2\sigma z}{\cos(\theta_i)}\right] \quad (9)$$

where σ is a coefficient defining the shape of the reflectivity function, interpreted as a mean extinction value.

The inversion of (7) with (8) and (9) using a single baseline is an underdetermined problem as the number of unknowns

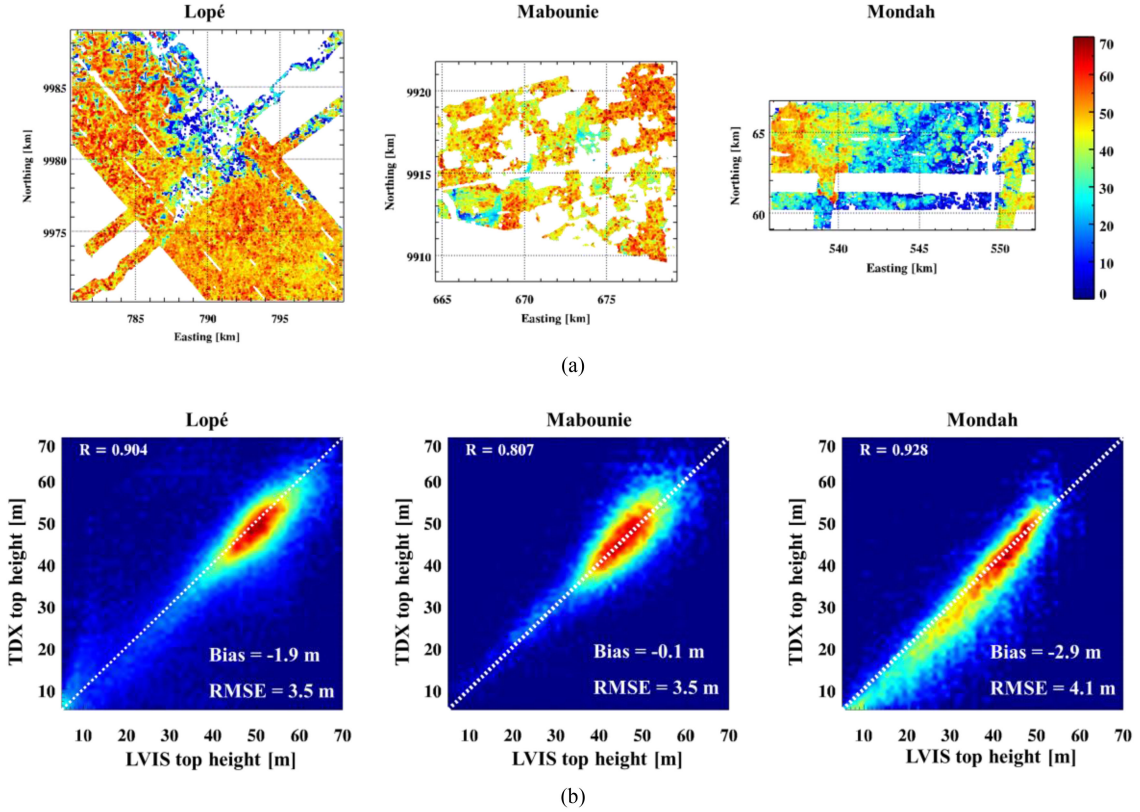


Fig. 4. (a) TanDEM-X top height (H_{TDX}) maps at 1 ha resolution, and (b) 2-D validation histograms against LVIS top heights (H_{LVIS}) for Lopé, Mabounie, and Mondah. The Pearson coefficient (R), bias, and RMSE are reported for each test sites.

(ϕ_0, h_V, σ) exceeds the number of measurements ($\gamma_{Vol}(\kappa_z)$). In this sense the use of an external DTM for calculating ϕ_0 has two advantages. First, it allows a balanced inversion. Second, it allows an unbiased estimation of h_V even if there is no penetration until the ground [35]. On the other hand, any offset (e.g., arising from residual TanDEM-X orbit errors) between ϕ_0 and $\gamma_{Vol}(\kappa_z)$ on surfaces must be compensated before the inversion [35].

The desired h_V is then obtained as the solution of [35]

$$\min_{h_V, \sigma} \|\gamma_{Vol}(\kappa_z) - \exp(i\phi_0) \cdot \gamma_V(\kappa_z; h_V, \sigma)\|. \quad (10)$$

Finally, similarly to the calculation of H_{LVIS} , the top height H_{TDX} is obtained by taking the maximum h_V for every 1 ha resolution cell on ground.

The inversion (10) was implemented and applied over the three sites using the LVIS DTMs to calculate ϕ_0 . The inversion was carried out only for $|\gamma_{Vol}(\kappa_z)| > 0.25$ with $\kappa_z < 0.12$ rad/m (HoA > 55 m) corresponding to 85% of the forested areas in Lopé, 90% in Mabounie and 100% in Mondah. The obtained maps of H_{TDX} and the 2-D histograms validating H_{TDX} against H_{LVIS} are shown in Fig. 4. The overall RMSE amounts to 3.5, 3.5, and 4.1 m, and the bias amounts to -1.9 , -0.1 , and -2.9 m in Lopé, Mabounie, and Mondah, respectively. For all the sites, H_{TDX} covers the same height range of H_{LVIS} , and the two height maps are well correlated. The lower coherence level in taller stands especially in Lopé and Mabounie increase the

standard deviation of H_{TDX} . H_{TDX} is clearly underestimated (i.e., has a negative bias) for $H_{LVIS} < 30$ m in Lopé and even more in Mondah probably as a result of an actually present ground scattering contribution, constituting a model mismatch in Lopé, heights are slightly underestimated also for $H_{LVIS} > 50$ m with a bias around -3 m. This is the effect of the relatively high κ_z that limits the sensitivity of the inversion for taller stands.

B. AGB Estimation Using Height

Here, the estimation of AGB by means of the height-to-biomass allometry is discussed. Using the LVIS height and biomass estimates the allometric level α_0 and the reference exponent β_0 of a height-to-biomass allometric relation with the form of (2) have been estimated by means of an ordinary least squares regression

$$\min_{\alpha_0, \beta_0} \left\| \mathbf{b}_{LVIS} - \alpha_0 \mathbf{h}_{LVIS}^{\beta_0} \right\|^2 \quad (11)$$

where \mathbf{b}_{LVIS} is a vector containing the biomass values B_{LVIS} and \mathbf{h}_{LVIS} contains the associated H_{LVIS} values. For each site, the regression has been performed individually accounting for the fact that certain height ranges may be insufficiently represented leading to $\alpha_0 = 0.473, 1.25, 3.4 \times 10^{-5}$ and $\beta_0 = 1.72, 1.44, 4.73$ for Lopé, Mabounie, and Mondah, respectively. While the allometric exponents in Lopé and Mabounie are similar, both of

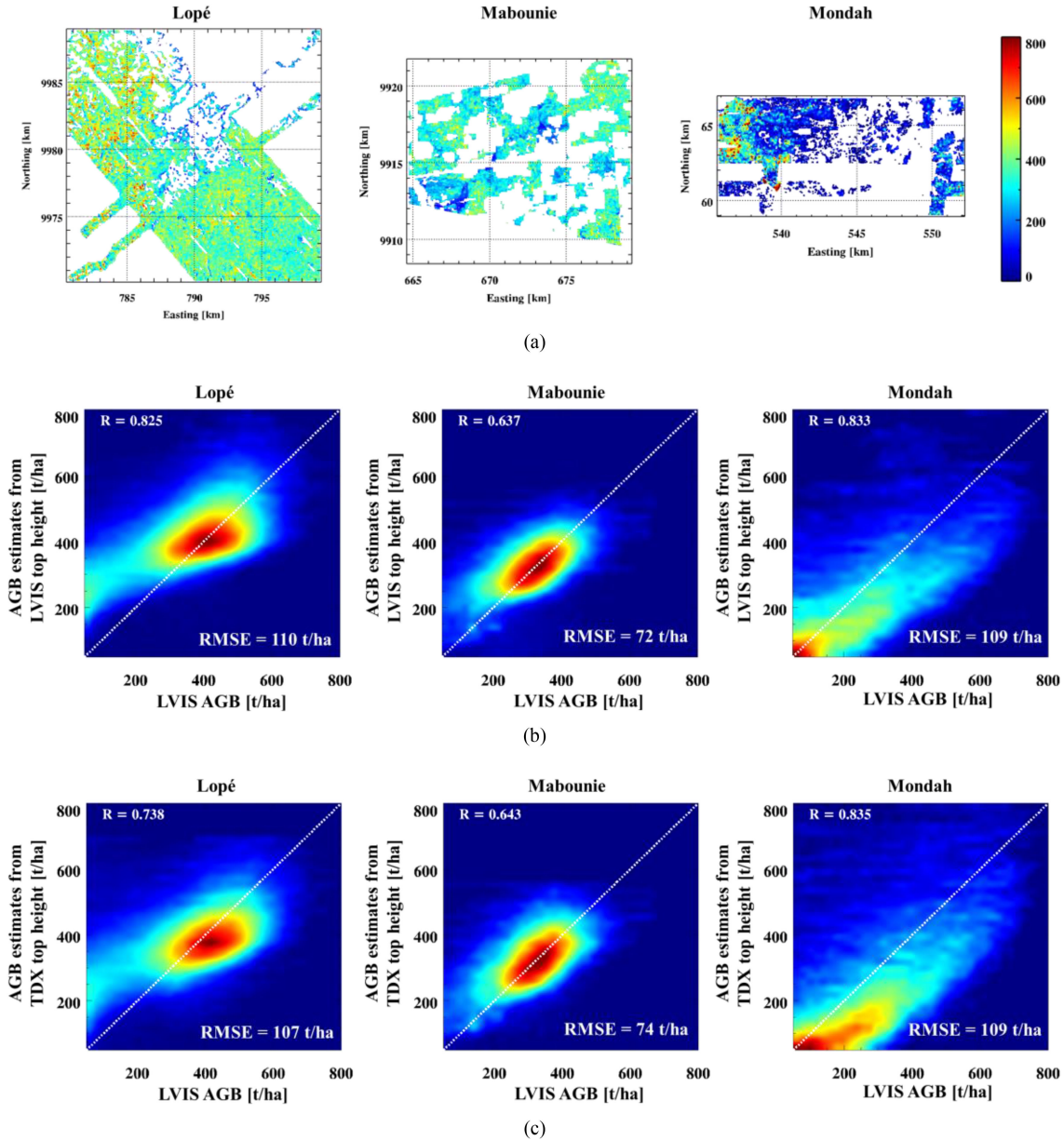


Fig. 5. (a) AGB maps (1 ha resolution) estimated from TanDEM-X top heights (H_{TDX}), and 2-D validation histograms of the biomass estimates against the reference biomass using. (b) LVIS top heights (H_{LVIS}). (c) TanDEM-X top heights (H_{TDX}) for Lopé, Mabounie, and Mondah. The overall estimation RMSE is reported.

them differ significantly from the one in Mondah. This probably reflects the large structural heterogeneity and presence of secondary and disturbed (open) forest stands in Mondah in contrast to the other two test sites.

After the definition of the height-to-biomass allometry, forest height estimates, either H_{TDX} or H_{LVIS} can be transformed to AGB estimates. The obtained AGB maps at 1 ha resolution are shown in Fig. 5. For all three sites the estimated AGB range is smaller than the LVIS AGB range: high AGB levels are consistently underestimated (by 100 t/ha or even more), especially in Lopé and Mondah. In contrast, low AGB levels tend to be overestimated, especially in Lopé and Mabounie. This behavior is common whether TanDEM-X or LVIS heights are used.

The insufficiency of a single allometric relation to describe accurately the height to biomass relationship even within a single site becomes apparent in the 2-D histograms of B_{LVIS} against H_{LVIS} plotted for each site in Fig. 6. The middle one of the three dotted lines indicates the height-to-biomass allometry as obtained from (11). In Lopé the AGB ranges from 350 up to 500 t/ha at a height of 50 m. A single height-to-biomass relationship cannot describe this spread. Two additional forest height-to-biomass allometries are plotted defined by the same reference allometric exponent and an allometric level increased (or decreased) by 30% with respect to the original one. It becomes clear that a smaller α_0 is able to compensate the overestimation of lower biomass levels (e.g., for sparse(r) stands) seen in Fig. 5. A larger α_0 fits better the higher AGB levels [e.g., for dense(r)

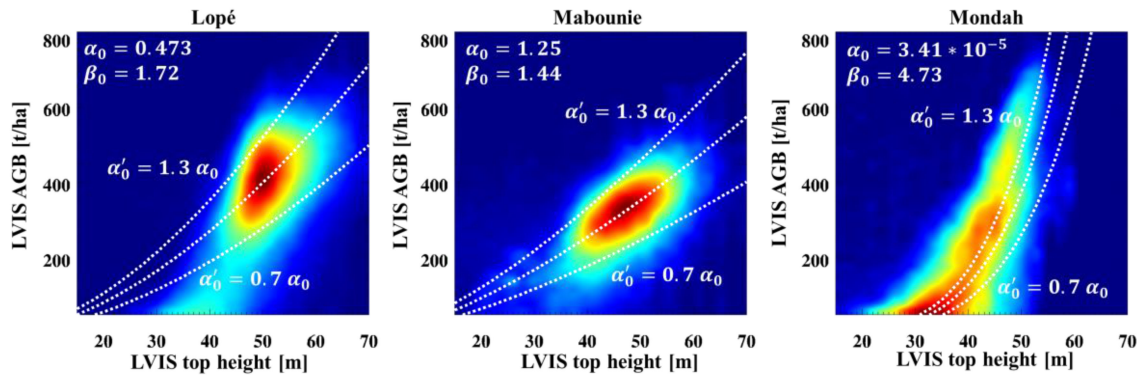


Fig. 6. 2-D histograms relating the LVIS top height (H_{LVIS}) and reference biomass (B_{LVIS}) at 1 ha resolution. Each dashed line represents a different height-biomass allometric relationship. The estimated allometric coefficients are reported.

stands] compensating their underestimation seen in Fig. 5. In conclusion, a single value of α_0 is not sufficient for an accurate biomass estimation. To account for this the use of a variable allometric level is attempted next.

IV. FOREST BIOMASS ESTIMATION FROM TANDEM-X HEIGHT AND HORIZONTAL STRUCTURE

A. Derivation of HS From TanDEM-X

The basic idea behind the structure estimation framework proposed in [23] and [24] is to quantify the variability in height of the top canopy “surface” from tomographically reconstructed 3-D reflectivity. In the case of TanDEM-X, where usually only one single-pass interferometric acquisition is available (with an appropriate vertical wavenumber), the reconstruction of a vertical reflectivity profile is not possible; at least not in a conventional tomographic way. However, the histogram of the interferometric phases (or alternatively of the converted phase center height) over a large enough area provides in many cases an approximation of the vertical reflectivity profiles [39]–[41]. Such profiles will be referred in the following as canopy height profiles (CHPs). Note that because of the different resolutions, the CHP can deviate significantly from the vertical reflectivity underlying the interferometric coherence. Nevertheless, the high attenuation at X-band combined with the high spatial resolution of the TanDEM-X interferograms support the correlation of phase center height variation to (top) canopy height variation allowing the use of the derived CHP to extract relevant horizontal structure information [41].

Interferometric coherences have been estimated with about 25 looks on a $10 \text{ m} \times 10 \text{ m}$ ground range-azimuth cell (see Section II). The LVIS DTM is converted to phase (by multiplying with the local vertical wavenumber) and subtracted from the interferometric phase in order to compensate any terrain-induced phase center variations. The obtained phase is then converted to phase center height (by dividing by the local vertical wavenumber). In this way, only the height variations induced by the canopy variability are relevant. Finally, vertical scattering profiles have been obtained within a $25 \text{ m} \times 25 \text{ m}$ cell. An example of such CHPs along a 1 km transect across the Lopé site is shown in Fig. 7 and compared with the corresponding

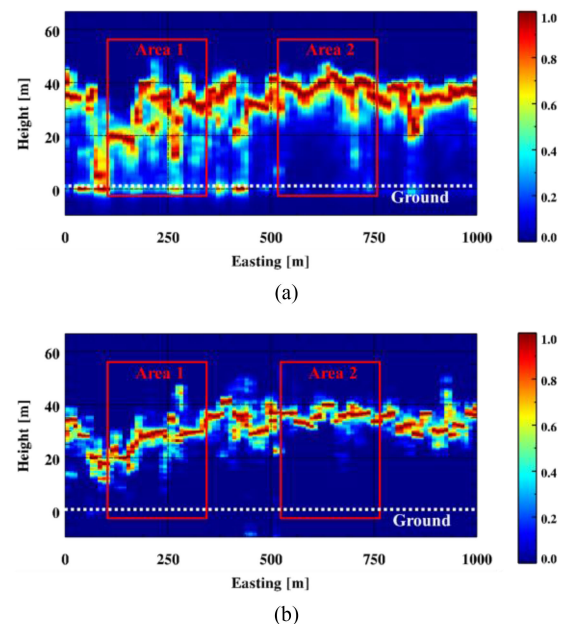


Fig. 7. Representative transects in Lopé at a constant northing coordinate. (a) LVIS waveforms. (b) TanDEM-X CHPs. Each profile is normalized by its maximum. The height axis is referred to the ground, which is located in its origin (0 m).

LVIS waveforms along the same transect. The peaks of the CHP are distributed closer to the canopy top, while the waveform peaks are distributed much wider between canopy top and the ground. Despite this difference, it is apparent that just based on the top canopy variability, the CHPs allow us to distinguish a sparser area (marked as “Area 1”) from a denser one (marked as “Area 2”).

With reference to Fig. 8, the calculation of the horizontal structure index HS proposed in [24] is based on “counting” the number of profile (i.e., reflectivity) peaks (associated to scattering contributions) located within a predefined top layer in a structure resolution cell. In practice, considering only the top layer allows us to separate the top canopy height variations from the (vertical) variations induced by volume scattering contributions [24]. As each CHP typically contributes with no

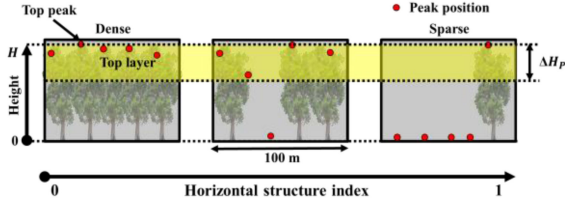


Fig. 8. Conceptual sketch related to the calculation of the horizontal structure index used in this article depicted on the three stands of Fig. 1.

more than a couple of peaks, the larger the number of peaks close to the canopy top, the more homogeneous is the forest height, and the higher is the local forest density. Referring the height of the highest peak in the structure resolution cell with H_P , the top height layer is defined as the fraction $\Delta \cdot H_P$ below H_P . The horizontal structure index is then calculated as [24]

$$HS = 1 - \frac{N_P}{N_{P, \max}} \quad (12)$$

where N_P is the number of CHP peaks in the top layer within the structure resolution cell, and $N_{P, \max}$ is a reference maximum often assumed as the maximum N_P within the site / scene. HS equals 0 in dense structure resolution cells, and 1 in sparse structure resolution cells corresponding to the cases illustrated in Fig. 8. The obtained HS value depends on the top layer extent: wider top layers contain more CHP peaks than thinner ones. As a consequence, the choice of an appropriate Δ is crucial for the ability of the index to reflect the physical structure (density) and its local variation.

Horizontal structure indices have been derived from the TanDEM-X CHPs and the LVIS waveforms (using the same waveform maxima counting procedure and same top layer as with the CHPs) denoted as HS_{TDX} and HS_{LVIS} , respectively. The CHPs have been additionally “multilooked” in height by means of a 10 m Gaussian-shaped moving window in order to suppress peaks caused by the (interferometric phase) noise. A (sliding) 1 ha structure resolution cell has been used to aggregate a statistically relevant number of CHP’s (or waveforms). Each structure resolution cell then contains 16 (4×4) profiles corresponding to non-overlapping areas on ground. A top layer extent $\Delta = 0.35$ has been chosen. This choice is rather empirical, although motivated by the analysis in [24]. However, both indices appear widely robust against the choice of the top layer extent: HS_{TDX} and HS_{LVIS} do not change significantly for Δ changing within 0.3 and 0.45, in accordance with the results reported in [41]. The derived HS_{TDX} and HS_{LVIS} maps for the three test sites are shown in Fig. 9 and reveal very similar structure patterns. In Lopé both indices distinguish the denser southeastern part from the sparser colonizing forest stands at the border to the savannah [30]. In Mabounie the mature forest stands are characterized as dense by both indices. Finally, Mondah’s disturbed open forest stands in the central part of the scene (indicated as sparse) are clearly distinguished from the older tall stands in the western part (indicated as dense) by both indices.

Fig. 10 shows the 2-D scatterplots of B_{LVIS} against H_{LVIS} for each site. The color of each point corresponds to its HS_{LVIS} value. Despite the dispersion, the dependency of the height-to-biomass allometry on the horizontal structure index HS_{LVIS} becomes clearly visible: for a given height level B_{LVIS} increases with decreasing HS_{LVIS} (i.e., with increasing forest density) or decreases with increasing HS_{LVIS} (i.e., with decreasing forest density). Interestingly, tall stands with top heights of about 40 m appear to have very low biomass levels (< 100 t/ha). Recalling the maps in Fig. 9, these stands are composed by few isolated tall trees and shorter vegetation, like for example the colonizing forest stands in Lopé or the sparse forest stands in the center of the Mondah site. This agrees with Fig. 6, and supports the idea of using the horizontal structure index to adapt α_0 on local stand conditions.

B. Biomass Estimation From TanDEM-X Forest Height and Horizontal Structure

In this Section, the improvement of the height-to-biomass allometry by exploring the dependency of the allometric level on the horizontal structure index is addressed.

To define the relation of the allometric level α_0 with the horizontal structure index HS the LVIS estimates B_{LVIS} , H_{LVIS} , and HS_{LVIS} are used. In the range from 0 to 1 HS_{LVIS} has been segmented into N_α nonoverlapping and uniformly distributed intervals centered around the structure values $\{HS_{LVIS,i}\}_{i=1}^{N_\alpha}$. For each of these intervals the allometric level $\{\alpha_0(HS_{LVIS,i})\}_{i=1}^{N_\alpha}$ and a common reference allometric exponent β_0 are jointly estimated by means of a least squares optimization, similarly to (11)

$$\min_{\{\alpha_0(HS_{LVIS,i})\}_{i=1}^{N_\alpha}, \beta_0} \left\| \begin{bmatrix} \mathbf{b}_{LVIS,1} \\ \vdots \\ \mathbf{b}_{LVIS,i} \\ \vdots \\ \mathbf{b}_{LVIS,N_\alpha} \end{bmatrix} - \begin{bmatrix} \alpha_0(HS_{LVIS,1}) \mathbf{h}_{LVIS,1}^{\beta_0} \\ \vdots \\ \alpha_0(HS_{LVIS,i}) \mathbf{h}_{LVIS,i}^{\beta_0} \\ \vdots \\ \alpha_0(HS_{LVIS,N_\alpha}) \mathbf{h}_{LVIS,N_\alpha}^{\beta_0} \end{bmatrix} \right\|^2 \quad (13)$$

where $\mathbf{b}_{LVIS,i}$ and $\mathbf{h}_{LVIS,i}$ are the vectors containing the (reference) B_{LVIS} and H_{LVIS} values, for the generic i th HS_{LVIS} interval centered at $HS_{LVIS,i}$. The obtained allometric exponents for the three test sites Lopé, Mabounie, and Mondah, are $\beta_0 = 1.8, 1.3$ and 2.5 , respectively. Note that the obtained reference allometric exponent β_0 are very similar (at least in Lopé and Mabounie), but not identical to the ones obtained from (11) as the two optimisation problems are different.

The general behavior of $\alpha_0(HS_{LVIS})$ is obtained from (2) by

$$\alpha_0(HS_{LVIS}) = \frac{B_{LVIS}}{H_{LVIS}^{\beta_0}} \quad (14)$$

and is visualized by means of a 2-D histogram in Fig. 11(a) for the Lopé site. The $\alpha_0(HS_{LVIS})$ obtained from (14) is indicated by the white dotted line. For all three sites a decreasing trend of $\alpha_0(HS_{LVIS})$ for increasing HS_{LVIS} is obtained. This agrees with

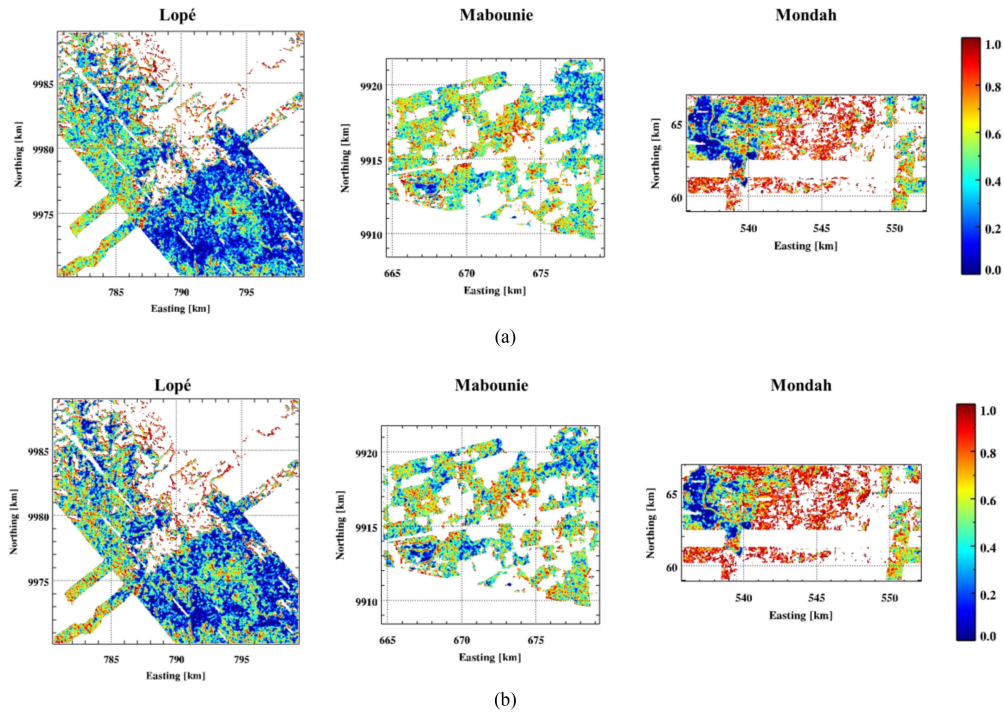


Fig. 9. Horizontal structure maps at 1 ha resolution (a) from LVIS waveforms (HS_{LVIS}) and (b) from TanDEM-X CHPs (HS_{TDX}) for Lopé, Mabounie, and Mondah. Sparse forest stands appears in red; dense stands appear in blue.

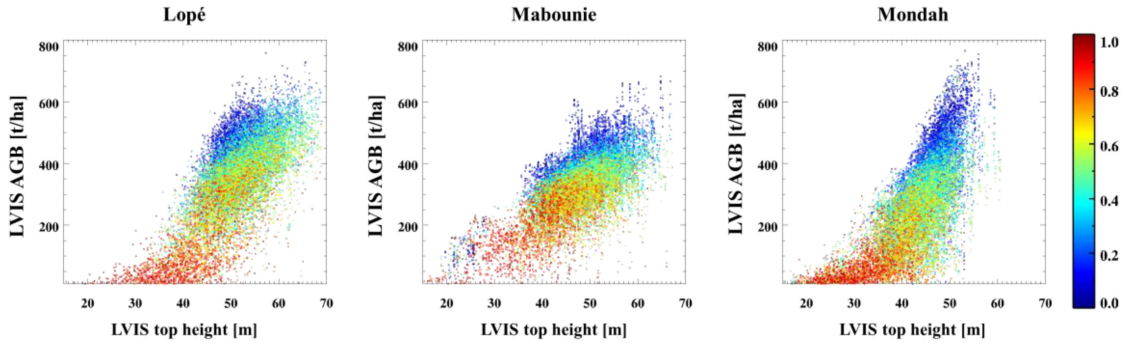


Fig. 10. Scatterplots between the reference LVIS top height (H_{LVIS}) and AGB (B_{LVIS}) for the three test sites. The color indicates the value of the LVIS horizontal structure index (HS_{LVIS}).

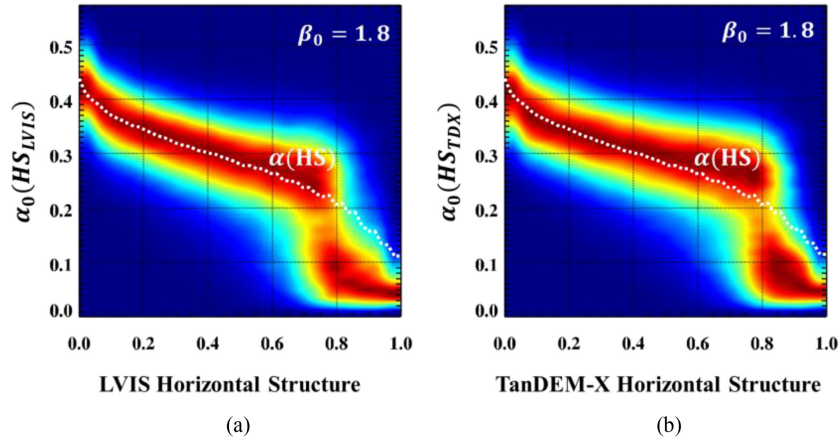


Fig. 11. 2-D histograms relating α_0 and horizontal structure from (a) LVIS waveforms (HS_{LVIS}). (b) TanDEM-X CHPs (HS_{TDX}) in Lopé with $\beta_0 = 1.8$. The white dashed line represents the horizontal structure function $\alpha(HS)$ estimated from the reference biomass and height maps as in (14).

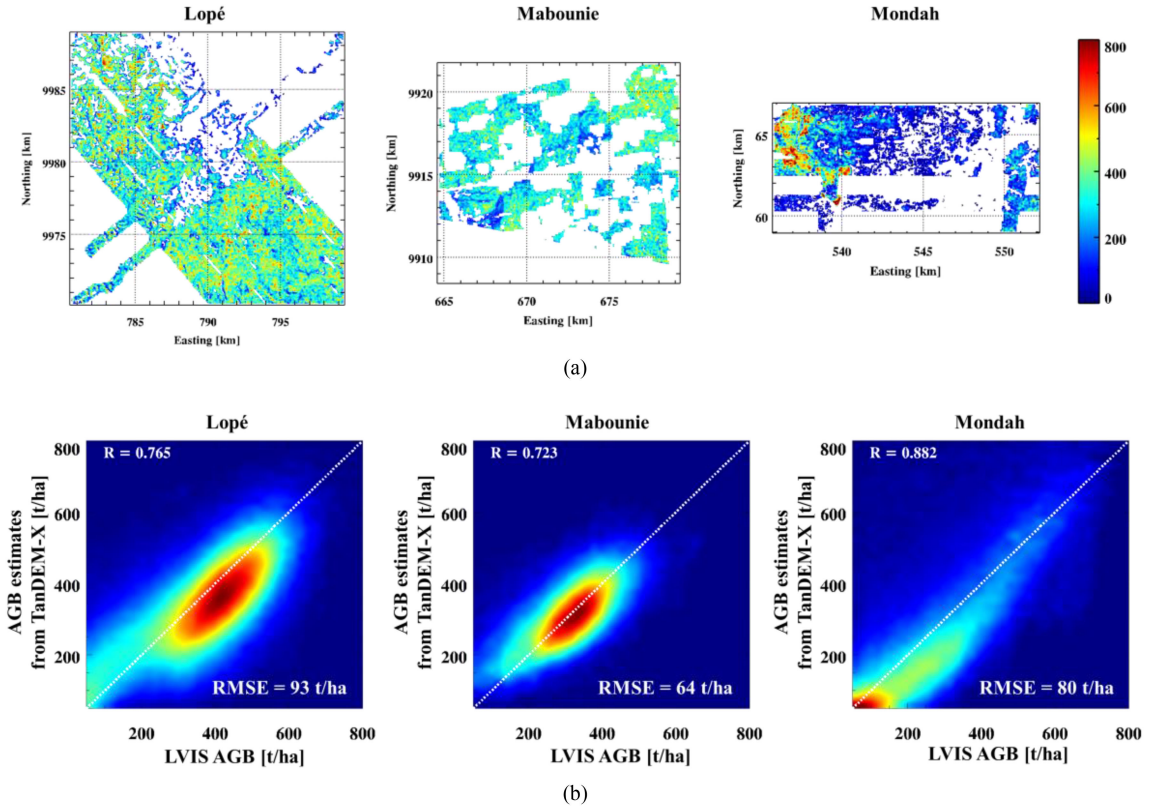


Fig. 12. (a) AGB maps from TanDEM-X top height (H_{TDX}) and structure (HS_{TDX}). (b) 2-D validation histograms of the TanDEM-X AGB estimates against the reference biomass (B_{LVIS}) for Lopé, Mabounie, and Mondah. The overall estimation RMSE is reported for each test sites.

Figs. 6 and 10, and confirms the relevance of the structure index for adjusting the allometric level. The distribution becomes wider for large HS_{LVIS} values (0.75 in Lopé, 0.9 in Mabounie and 0.75 in Mondah). At larger HS_{LVIS} levels, $\alpha_0(HS_{LVIS})$ jumps suddenly to very small values, and its distribution becomes asymmetrical. If HS_{TDX} is used instead of HS_{LVIS} , the distribution of $\alpha_0(HS_{TDX})$ [see Fig. 11(b)] becomes slightly wider, but its behavior does not change significantly.

AGB could be estimated by using H_{TDX} and $\alpha_0(HS_{TDX})$ in (3). The validation of the obtained AGB against the LVIS AGB are shown in Fig. 12. It becomes clear that the use of $\alpha_0(HS_{TDX})$ successfully compensates for the density and/or structure induced variation of the single allometry with fixed allometric level. Indeed, the estimation performance increases drastically: the RMSE decreases down to 15%–25% while the correlation coefficient increases to up to 0.7–0.9 for the different sites. The strong overestimation especially for low biomass values in Fig. 5 is widely compensated. The remaining residual overestimation, especially in Lopé, is a result of the ambiguity to relate α_0 to a single value of HS_{TDX} at large HS values (see Fig. 11). The optimization of (13) is equivalent to a minimization of the mean square error, including both the estimation bias and the standard deviation. Choosing $\alpha_0(HS)$ as the one minimizing the bias between the estimates and LVIS AGB compensates almost complete the bias in the low biomass regions at the cost of an overall increase of the RMSE by 10%. However, AGB can still be underestimated in the high biomass region as a result of the underestimation of forest height.

C. Common Height and Structure-to-Biomass Allometry Across Test Sites

The generalization of the height-to-biomass allometry across the three sites requires the estimation of a common (constant) allometric exponent β_{0C} and a common $\alpha_{0C}(HS_{TDX})$ relation for all sites. For this, the procedure outlined in Sections IV-B has been applied to 50000 B_{LVIS} , H_{LVIS} , and HS_{LVIS} samples from all three sites. The samples are randomly selected across biomass levels in order to equally represent each site. In this way, an allometric exponent of $\beta_{0C} = 1.7$ and the $\alpha_{0C}(HS_{TDX})$ relationship shown in Fig. 13(a) are obtained. The behavior of $\alpha_{0C}(HS_{TDX})$ is consistent to the single-site relations obtained in the following section. The AGB estimates obtained from the common allometry and its comparison with the reference AGB is shown in Fig. 13(b). The overall RMSE is about 79 t/ha while the correlation is larger than 0.8. An underestimation of about 50 t/ha appears at around 300 t/ha. The overall performance is however convincing, keeping in mind the very different characteristics of the three sites.

D. Effect of Reduced Penetration on Structure Calculation

TanDEM-X forest height estimation is limited by the insufficient penetration capability at X-band due to the high attenuation rates especially in tall/dense/wet forest conditions. This limitation no longer exists if the ground topography is known (e.g., an external DTM is available). In this sense, the lack of a DTM

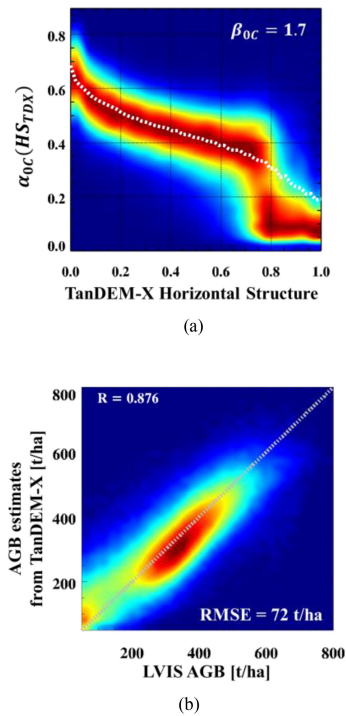


Fig. 13. Common height and structure-to-biomass allometry across test sites. (a) Horizontal structure function $\alpha_{0C}(HS)$ with $\beta_{0C} = 1.7$. (b) 2-D validation histogram of the TanDEM-X AGB estimates against reference biomass (B_{LVIS}).

becomes critical for forest height estimation in tall/dense/wet forest conditions. Different height estimation algorithms can be followed [42]. Any additional height estimation inaccuracy resulting from this is directly reflected into an additional inaccuracy of B_{TDX} . By differentiating (3), it is readily found that the sensitivity of a biomass estimation error is directly proportional to $\alpha_0(HS_{TDX})$. From Figs. 11 or 13, it is apparent that a height error induces a larger biomass error for smaller HS_{TDX} (i.e., denser forest stands) for a fixed allometric exponent.

With respect to the horizontal structure index, the high attenuation rates become an advantage increasing the sensitivity to the top-canopy height variations. Therefore, it is expected that the unavailability of an external DTM is less critical for its estimation [15], [41]. The external DTM allows us to separate the top-canopy height variations from the topographic induced height variations. However, as the two contributions are expected to occur at different spatial scales this may allow us to separate them from each other. As reported in an earlier study a low resolution TanDEM-X DEM can be used to compensate topographic induced height variations with sufficient accuracy [43]. A spatial resolution in the order of 100 m appears optimum [15], [43]. After DEM phase compensation both the CHP and the HS_{TDX} are estimated as described.

In order to test the validity of these expectations HS_{TDX} calculated with and without DTM are compared in Fig. 14. In order to increase the significance of this comparison the same top layer width has been used. The good agreement obtained in all sites confirms that the reduced penetration is the key feature for the retrieval of structure information. The availability of a DTM plays only a secondary role. However, it can still lead to a loss of performance especially in areas characterized by

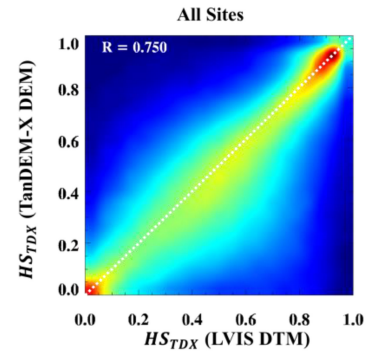


Fig. 14. Two-dimensional histograms relating HS_{TDX} across test sites obtained using the LVIS DTM (horizontal axis) and the TanDEM-X low resolution DEM (vertical axis) as references for the phase center heights.

small-scale topographic variations as it has been seen in Lopé and Mabounie.

It is worth remarking that in the used structure estimation framework an error in the top layer width becomes a (relative) error in HS_{TDX} . HS_{TDX} increases for an underestimated width as the top layer includes more CHP peaks, and vice versa. In this sense, compared to the knowledge of the ground topography, the misidentification of the top layer can cause a larger performance degradation. However, as discussed above, the performance remains comparable even for significant variations (50%) of the selected top layer.

V. CONCLUSION

The potential of using forest structure information to adapt a general height-to-biomass allometry to local stand conditions for improving biomass estimation performance is investigated. It is addressed in terms of forest height and structure indices derived from remote sensing measurements particularly in the TanDEM-X context.

The discussed concepts have been demonstrated and validated with TanDEM-X data acquired in 2015–2016 over three different test sites in Gabon in the frame of the AfriSAR campaign. Reference forest height and biomass data as well as (horizontal) forest structure indices have been derived from airborne (LVIS) full waveform data acquired almost at the same time as the TanDEM-X data. TanDEM-X forest height, structure index and biomass estimates have been derived at a spatial scale of 1 ha and compared against the lidar reference data. The general height-to-biomass allometry used to transform forest height estimates to biomass has been established using the lidar height and biomass estimates. The lidar (LVIS) DTM has been used to compensate for the interferometric phase component induced by the terrain topography supporting in this way both the forest height inversion and the estimation of the horizontal structure index from TanDEM-X data.

Forest top height has been estimated with an RMSE well within 20%. In contrast, the biomass values obtained from a single height-to-biomass allometry is affected by large biases independently of the height estimation error.

A continuous relationship between the allometric level and the horizontal structure index was derived by means of a least

squares minimization of the biomass RMSE. The achieved results indicate that the horizontal structure index is able to adapt a more general height-to-biomass relation to local forest (density) conditions by changing the allometric level. The estimation biases appearing in the conventional single height-to-biomass allometry are widely compensated improving the overall biomass RMSE up to 30%. In addition, the ability to establish a common height-to-biomass allometry supported by the horizontal structure index for all three sites with a reasonable performance is an important result. The identification of the top canopy layer in which the height variability is evaluated remains a critical choice in the estimation of the horizontal structure index.

Regarding the role of the lidar data, they are indispensable for the definition of the forest height-to-biomass allometry. However, their role in the estimation of forest height and the horizontal structure index is less critical as both can be performed even in the absence of any lidar measurements. More affected from the lack of lidar measurements is the estimation of forest height in tall/dense/wet forest conditions due to the high attenuation at X-band [42], rather than the estimation of the horizontal structure index itself.

There are three important features that make TanDEM-X especially appropriate for the quantitative characterization of the horizontal forest structure: the high attenuation rates at X-band and the associated limited penetration into the forest volume that maximize the sensitivity of the TanDEM-X (complex) coherence to the spatial variability of the top canopy layer; the high interferometric accuracy of TanDEM-X (driven by the single-pass implementation) that allows us to capture the structure induced (complex) coherence variation; and the high spatial resolution of the TanDEM-X (complex) coherence measurements and its continuous measurement nature allows the estimation of structure induced variations at spatial scales relevant for the characterization of the horizontal forest structure.

ACKNOWLEDGMENT

The lidar AfriSAR datasets were provided by the land, vegetation, and ice sensor team in Code 61A at NASA Goddard Space Flight Center with support from the University of Maryland, College Park, MD, USA. This work was performed in the frame of a joint research project between DLR and NASAs carbon monitoring system (CMS) program in support of NASA Grant #80NSSC20K0023 to the University of Maryland.

REFERENCES

- [1] R. A. Houghton, F. Hall, and S. J. Goetz, "Importance of biomass in the global carbon cycle," *J. Geophys. Res.-Biogeosci.*, vol. 114, 2009, Art. no. G00E03.
- [2] M. Reichstein and N. Carvalhais, "Aspects of forest biomass in the earth system: Its role and major unknowns," *Surv. Geophys.*, vol. 40, no. 4, pp. 693–707, Jul. 2019.
- [3] J. Chave *et al.*, "Tree allometry and improved estimation of carbon stocks and balance in tropical forests," *Oecologia*, vol. 145, no. 1, pp. 87–99, 2005.
- [4] T. Mette, K. Papathanassiou, I. Hajnsek, H. Pretzsch, and P. Biber, "Applying a common allometric equation to convert forest height from Pol-InSAR data to forest biomass," in *Proc. IEEE Int. Geosci. Remote Sens. Symp.*, 2004, pp. 269–272.
- [5] G. P. Asner *et al.*, "A universal airborne LiDAR approach for tropical forest carbon mapping," *Oecologia*, vol. 168, no. 4, pp. 1147–1160, Apr. 2012.
- [6] T. Mette, K. Papathanassiou, and I. Hajnsek, "Biomass estimation from polarimetric SAR interferometry over heterogeneous forest terrain," in *Proc. IEEE Int. Geosci. Remote Sens. Symp.*, 2004, pp. 511–514.
- [7] A. Torano Caicoya, F. Kugler, I. Hajnsek, and K. Papathanassiou, "Large-scale biomass classification in boreal forests with TanDEM-X data," *IEEE Trans. Geosci. Remote Sens.*, vol. 54, no. 10, pp. 5935–5951, Oct. 2016.
- [8] N. Knapp, R. Fischer, and A. Huth, "Linking lidar and forest modeling to assess biomass estimation across scales and disturbance states," *Remote Sens. Environ.*, vol. 205, Feb. 2020, Art. no. 111597.
- [9] N. Knapp, R. Fischer, V. Cazcarra-Bes, and A. Huth, "Structure metrics to generalize biomass estimation from lidar across forest types from different continents," *Remote Sens. Environ.*, vol. 237, pp. 199–209, Feb. 2020.
- [10] M. Schlund, S. Erasmí, and K. Scipal, "Comparison of aboveground biomass estimation from InSAR and LiDAR canopy height models in tropical forests," *IEEE Geosci. Remote Sens. Lett.*, vol. 17, no. 3, pp. 367–371, Mar. 2020.
- [11] M. J. Soja, H. J. Persson, and L. M. H. Ulander, "Estimation of forest biomass from two-level model inversion of single-pass InSAR data," *IEEE Trans. Geosci. Remote Sens.*, vol. 53, no. 9, pp. 5083–5099, Sep. 2015.
- [12] A. E. L. Stovall and H. H. Shugart, "Improved biomass calibration and validation with terrestrial lidar: Implications for future LiDAR and SAR missions," *IEEE J. Sel. Topics Appl. Earth Observ. Remote Sens.*, vol. 11, no. 10, pp. 3527–3537, Oct. 2018.
- [13] J. B. Drake *et al.*, "Estimation of tropical forest structure characteristics using large-footprint lidar," *Remote Sens. Environ.*, vol. 79, no. 2/3, pp. 305–319, Feb. 2002.
- [14] R. O. Dubayah *et al.*, "Estimation of tropical forest height and biomass dynamics using lidar remote sensing at La Selva, Costa Rica," *J. Geophys. Res.*, vol. 115, no. G2, 2010.
- [15] E. C. De Grandi, E. Mitchard, and D. Hoekman, "Wavelet based analysis of TanDEM-X and LiDAR DEMs across a tropical vegetation heterogeneity gradient driven by fire disturbance in Indonesia," *Remote Sens.*, vol. 8, no. 8, pp. 641–667, Aug. 2016.
- [16] P. Da Conceição Bispo *et al.*, "Mapping forest successional stages in the Brazilian Amazon using forest heights derived from TanDEM-X SAR interferometry," *Remote Sens. Environ.*, vol. 232, Jul. 2019, Art. no. 111194.
- [17] S. Erasmí, M. Semmler, P. Schall, and M. Schlund, "Sensitivity of bistatic TanDEM-X data to stand structural parameters in temperate forests," *Remote Sens.*, vol. 11, Dec. 2019, Art. no. 2966.
- [18] J. I. H. Askne, H. J. Persson, and L. M. H. Ulander, "On the sensitivity of TanDEM-X observations to boreal forest structure," *Remote Sens.*, vol. 11, Dec. 2019, Art. no. 1644.
- [19] M. J. Soja, H. J. Persson, and L. M. H. Ulander, "Estimation of forest height and canopy density from a single InSAR correlation coefficient," *IEEE Geosci. Remote Sens. Lett.*, vol. 12, no. 3, pp. 646–650, Mar. 2015.
- [20] S. Solberg, E. H. Hansen, T. Gobakken, E. Naesset, and E. Zahabu, "Biomass and InSAR height relationship in a dense tropical forest," *Remote Sens. Environ.*, vol. 192, pp. 166–175, Apr. 2017.
- [21] R. Treuhaft *et al.*, "Tropical-forest structure and biomass dynamics from TanDEM-X radar interferometry," *Forests*, vol. 8, no. 8, Jul. 2017.
- [22] A. Torano Caicoya, M. Pardini, I. Hajnsek, and K. Papathanassiou, "Forest above-ground biomass estimation from vertical reflectivity profiles at L-band," *IEEE Geosci. Remote Sens. Lett.*, vol. 12, no. 12, pp. 2379–2383, Dec. 2015.
- [23] V. Cazcarra Bes, M. Tello Alonso, R. Fischer, M. Heym, and K. Papathanassiou, "Monitoring of forest structure dynamics by means of L-band SAR tomography," *Remote Sens.*, vol. 9, no. 12, pp. 1229–1250, Nov. 2017.
- [24] M. Tello Alonso, V. Cazcarra Bes, M. Pardini, and K. Papathanassiou, "Forest structure characterization from SAR tomography at L-band," *IEEE J. Sel. Topics Appl. Earth Observ. Remote Sens.*, vol. 11, no. 10, pp. 3402–3414, Oct. 2018.
- [25] M. Pardini *et al.*, "Early lessons on combining lidar and multi-baseline SAR Measurements for forest structure characterization," *Surv. Geophys.*, vol. 40, no. 4, pp. 803–837, Jul. 2019.
- [26] L. Reineke, "Perfecting a stand-density index for even aged forests," *J. Agricultural Res.*, vol. 46, no. 7, pp. 627–638, 1933.
- [27] I. Hajnsek *et al.*, "Technical assistance for the development of airborne SAR and geophysical measurements during the AfriSAR campaign." Final technical report, ESA contract no. 4000114293/15/NL/CT. [Online]. Available: <https://earth.esa.int/documents/10174/134665/AfriSAR-Final-Report>

- [28] L. Fatoyinbo *et al.*, “The NASA AfriSAR campaign: Airborne SAR and lidar measurements of tropical forest structure and biomass in support of future space missions,” *Remote Sens. Environ.*, vol. 264, 2021, Art. no. 112533.
- [29] N. Labriere *et al.*, “In situ reference datasets from the TropiSAR and AfriSAR campaigns in support of upcoming spaceborne biomass missions,” *IEEE J. Sel. Topics Appl. Earth Observ. Remote Sens.*, vol. 11, no. 10, pp. 3617–3627, Oct. 2018.
- [30] S. M. Marselis, H. Tang, J. D. Armston, K. Calders, N. Labrière, and R. Dubayah, “Distinguishing vegetation types with airborne waveform lidar data in a tropical forest-savanna mosaic: A case study in Lopé National Park, Gabon,” *Remote Sens. Environ.*, vol. 216, pp. 626–634, Oct. 2018.
- [31] E. T. A. Mitchard *et al.*, “Mapping tropical forest biomass with radar and spaceborne LiDAR in Lopé National Park, Gabon: Overcoming problems of high biomass and persistent cloud,” *Biogeosciences*, vol. 9, no. 1, pp. 179–191, Jan. 2012.
- [32] J. B. Blair and M. Hofton, AfriSAR LVIS L1B geolocated return energy waveforms, version 1, NASA National Snow and Ice Data Center Distributed Active Archive Center, Boulder, CO USA, 2018, doi: [10.5067/ED51YGVTB50Z](https://doi.org/10.5067/ED51YGVTB50Z).
- [33] J. B. Blair and M. Hofton, AfriSAR LVIS L2 geolocated surface elevation product, version 1, NASA National Snow and Ice Data Center Distributed Active Archive Center, Boulder, CO USA, 2018, doi: [10.5067/A0PMUXVUYNH](https://doi.org/10.5067/A0PMUXVUYNH).
- [34] J. Armston *et al.*, AfriSAR: Gridded forest biomass and canopy metrics derived from LVIS, Gabon, Oak Ridge National Laboratory Distributed Active Archive Center DAAC, Oak Ridge, TN, USA, 2016, doi: [10.3334/ORNLDAAC/1775](https://doi.org/10.3334/ORNLDAAC/1775).
- [35] F. Kugler, D. Schulze, I. Hajnsek, H. Pretzsch, and K. Papathanassiou, “TanDEM-X Pol-InSAR performance for forest height estimation,” *IEEE Trans. Geosci. Remote Sens.*, vol. 52, no. 10, pp. 6404–6422, Oct. 2014.
- [36] F. Kugler, S. K. Lee, I. Hajnsek, and K. P. Papathanassiou, “Forest height estimation by means of Pol-InSAR data inversion: The role of the vertical wavenumber,” *IEEE Trans. Geosci. Remote Sens.*, vol. 53, no. 10, pp. 5294–5311, Oct. 2015.
- [37] M. Martone, B. Bräutigam, P. Rizzoli, C. Gonzalez, M. Bachmann, and G. Krieger, “Coherence evaluation of TanDEM-X interferometric data,” *ISPRS J. Photogramm. Remote Sens.*, vol. 73, pp. 21–29, Sep. 2012.
- [38] K. Papathanassiou and S. R. Cloude, “Single-baseline polarimetric SAR interferometry,” *IEEE Trans. Geosci. Remote Sens.*, vol. 39, no. 11, pp. 2352–2363, Nov. 2001.
- [39] R. N. Treuhaft *et al.*, “Vegetation profiles in tropical forests from multi-baseline interferometric synthetic aperture radar, field, and lidar measurements,” *J. Geophys. Res.*, vol. 114, 2009.
- [40] R. N. Treuhaft *et al.*, “Exploring vegetation profiles from TanDEM-X phase, Lidar, and field measurements in tropical forests,” in *Proc. 10th Eur. Conf. Synthetic Aperture Radar*, 2014, pp. 1–3.
- [41] A. Pulella *et al.*, “Tropical forest structure observation with TanDEM-X data,” in *Proc. IEEE Int. Geosci. Remote Sens. Symp.*, 2017, pp. 918–921.
- [42] R. Guliaev, V. Cazcarra-Bes, M. Pardini, and K. Papathanassiou, “Forest height estimation by means of TanDEM-X InSAR and waveform lidar data,” *IEEE J. Sel. Topics Appl. Earth Observ. Remote Sens.*, vol. 14, pp. 3084–3094, 2021.
- [43] C. Choi, M. Pardini, and K. Papathanassiou, “Quantification of horizontal forest structure from high resolution TanDEM-X interferometric coherences,” in *Proc. IEEE Int. Geosci. Remote Sens. Symp.*, 2018, pp. 376–379.



Matteo Pardini (Member, IEEE) received the M.Eng. degree (*summa cum laude*) in telecommunication engineering and the Ph.D. degree in information engineering from the University of Pisa, Pisa, Italy, in 2006 and 2010, respectively.

In January 2010, he was with Information Retrieval Group, Radar Concepts Department, Microwaves and Radar Institute, Deutsches Zentrum für Luft- und Raumfahrt, Oberpfaffenhofen, Cologne, Germany, as a Research Scientist, after a visiting research period from August to December 2009. In 2017, he was a Visiting Scientist with the Department of Geographical Sciences, University of Maryland, College Park, MD, USA. His research interests include synthetic aperture radar (SAR) tomographic and polarimetric interferometric processing for three-dimensional bio/geophysical information extraction over natural volumes (forest, agriculture, and ice), SAR mission design, and SAR mission performance analysis.

Dr. Pardini is a member of DLRs TanDEM-X and Tandem-L science teams. He was the recipient of with IEEE GRSS IEEE GRSS J-STARS Paper Award in 2019 and the DLR Science Award in 2020.



Michael Heym received the Dipl. Ing. degree in forestry in 2006 from Eberswalde University for Sustainable Development, Eberswalde, Germany, and the M.Sc. degree in forest information technology from Eberswalde University, Eberswalde, Germany, for sustainable development as well as from the Warsaw University of Life Sciences, Warsaw, Poland. He is currently working toward the Ph.D. degree with Technische Universität München, Munich, Germany.

From 2010 to 2020, he was with the Chair of Forest Growth of Yield Science, Technische Universität München. Since 2020, he has been with the Department of Silviculture and Mountain Forests, Bavarian State Institute of Forestry, Freising, Germany, jointly responsible for the Fourth National Forest Inventory in Bavaria. He is further interested in linking forest structural information with remote sensing related datasets. His research interests include forest inventory data with respect to growth and yield as well as linking them to biodiversity related aspects.



Konstantinos P. Papathanassiou (Fellow, IEEE) received the Dipl. Ing degree in 1994 and the doctoral degree in 1999 from the Technical University of Graz, Graz, Austria.

From 1992 to 1994, he was with the Institute for Digital Image Processing of Joanneum Research, Graz, Austria. Between 1995 and 1999, he was with Microwaves and Radar Institute (HR), German Aerospace Center (DLR), Oberpfaffenhofen, Germany. From 1999 to 2000, he was an EU Post-Doctoral Fellow with Applied Electromagnetics, St.

Andrews, Scotland. Since October 2000, he has been with Microwaves and Radar Institute (HR), DLR. He is a Senior Scientist leading the Information Retrieval Research Group, DLR-HR. He is a member of DLR’s TanDEM-X and Tandem-L science teams, JAXA’s ALOS-PalSAR Cal-Val teams, ESA’s BIOMASS Mission Advisory Group and JAXA’s Carbon and Kyoto Initiative, and NASA’s GEDI Mission Science Team. He has more than 60 peer-reviewed articles in international journals and of more than 300 contributions in international conferences and workshops. His main research interests include polarimetric and interferometric processing and calibration techniques, polarimetric SAR interferometry, and the quantitative parameter estimation from SAR data, as well as in SAR mission design and SAR mission performance analysis.

Dr. Papathanassiou was the recipient of the IEEE GRSS IGARSS Symposium Prize Paper Award in 1998, the Best Paper Award of the European SAR Conference (EUSAR) in 2002, the IEEE GRSS J-STARS Paper Award in 2019, the DLR Science Award in 2002 and 2020, the DLR’s Senior Scientist Award in 2011 and the IEEE Fellow Award in 2015 and DLR’s Otto Lilienthal Award in 2020.



Changhyun Choi received the B.S. and M.S. degrees in earth and environmental sciences from Seoul National University, Seoul, South Korea, in 2014 and 2017, respectively. He is currently working toward the Ph.D. degree with Information Retrieval Research Group, Microwaves and Radar Institute, Deutsches Zentrum für Luft- und Raumfahrt, Cologne, Germany.

His main research interests include synthetic aperture radar signal processing for forest applications, focusing the retrieval of forest structural parameters

from interferometric SAR data.